NANO · MICRO small
www.small-journal.com

Check for updates

Direct Evidence of Lithium Ion Migration in Resistive Switching of Lithium Cobalt Oxide Nanobatteries

*Van Son Nguyen, Van Huy Mai, Pascale Auban Senzier, Claude Pasquier, Kang Wang, Marcelo J. Rozenberg, Nathalie Brun, Katia March, François Jomard, John Giapintzakis, Cristian N. Mihailescu, Evripides Kyriakides, Pavan Nukala, Thomas Maroutian, Guillaume Agnus, Philippe Lecoeur, Silvia Matzen, Pascal Aubert, Sylvain Franger, Raphaël Salot, Pierre-Antoine Albouy, David Alamarguy, Brahim Dkhil, Pascal Chrétien, and Olivier Schneegans**

Lithium cobalt oxide nanobatteries offer exciting prospects in the field of nonvolatile memories and neuromorphic circuits. However, the precise underlying resistive switching (RS) mechanism remains a matter of debate in two-terminal cells. Herein, intriguing results, obtained by secondary ion mass spectroscopy (SIMS) 3D imaging, clearly demonstrate that the RS mechanism corresponds to lithium migration toward the outside of the Li_xCoO_2 layer. These observations are very well correlated with the observed insulator-to-metal transition of the oxide. Besides, smaller device area experimentally yields much faster switching kinetics, which is qualitatively well accounted for by a simple numerical simulation. Write/erase endurance is also highly improved with downscaling – much further than the present cycling life of usual lithium-ion batteries. Hence very attractive possibilities can be envisaged for this class of materials in nanoelectronics.

1. Introduction

Redox-based nanoionic resistive memories (ReRAM) are memristive systems[1–3] which appear as highly promising candidates toward both nanoscale information storage and neuromorphic computing.[4] However, the attainable progress of ReRAM is contingent on a better understanding of the underlying mechanisms, thereby allowing precise control of resistive switching (RS) characteristics (switching speed, endurance etc.). The redox mechanisms observed in ReRAM are often based on the formation/rupture of conducting filaments, involving either metal cations (mechanisms referred to

Dr. V. S. Nguyen, Dr. D. Alamarguy, P. Chrétien, Dr. O. Schneegans
Laboratoire de Génie Electrique et Electronique de Paris
CNRS, CentraleSupélec, Universités UPMC et Paris-Sud
11 rue Joliot-Curie, 91192 Gif-sur-Yvette, France
E-mail: schneegans@geeps.centralesupelec.fr

Dr. V. H. Mai
Department of Optical Electronic Devices
Le Quy Don Technical University
236 Hoang Quoc Viet
Hanoi, Vietnam

Dr. P. Auban Senzier, Prof. C. Pasquier, Dr. K. Wang, Dr. M. J. Rozenberg, Dr. N. Brun, Dr. K. March, Dr. P.-A. Albouy
Laboratoire de Physique des Solides
Université Paris-Sud
bât 510, 91405 Orsay, France

Dr. F. Jomard
Groupe d'Étude de la Matière Condensée
Université de Versailles Saint-Quentin-En-Yvelines
Bat Fermat, 45 Avenue des Etats-Unis
78035 Versailles, France

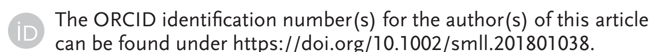
The ORCID identification number(s) for the author(s) of this article can be found under https://doi.org/10.1002/smll.201801038.

DOI: 10.1002/smll.201801038

Prof. J. Giapintzakis, Dr. C. N. Mihailescu, Dr. E. Kyriakides
Department of Mechanical and Manufacturing Engineering
University of Cyprus
75 Kallipoleos Avenue, PO Box 20537
1678 Nicosia, Cyprus

Dr. C. N. Mihailescu
National Institute for Laser
Plasma and Radiation Physics
409 Atomistilor Street, PO Box MG-36, 077125 Magurele, Romania

Dr. P. Nukala, Dr. B. Dkhil
Laboratoire Structures, Propriétés et Modélisation des Solides
CentraleSupélec
3 rue Joliot-Curie
91190 Gif-Sur-Yvette, France

Dr. T. Maroutian, Dr. G. Agnus, Prof. P. Lecoeur, Dr. S. Matzen, Prof. P. Aubert
Centre de Nanosciences et de Nanotechnologies
CNRS et Université Paris-Sud
Bât 220, rue André Ampère
91405 Orsay, France

Prof. S. Franger
Institut de Chimie Moléculaire et des Matériaux d'Orsay
Bât 410, rue du doyen Georges Poitou
91405 Orsay, France

© 2018 WILEY-VCH Verlag GmbH & Co. KGaA, Weinheim

as electrochemical metallization memories (ECM)) or oxygen vacancies.[5,6]

Apart from this, a new promising class of Li-based RS materials has recently been observed.[7–12] Such a class, which embodies oxide-based RS devices for memristive systems with Li-based nanobatteries, is of substantial technological relevance to the state-of-the-art. The possibility of combining nonvolatile resistive switching and charge modulation – more specific of the behavior of neurons[13]—ushers in a new dimension of control and functionalities.

However, the actual switching mechanism is still a matter of debate in two terminals E1/Li-based oxide/E2 devices (where E1 and E2 represent electrodes). It has been proposed that it may be related to the formation/rupture of lithium filaments inside the oxide layer[14] (thus belonging to ECM-based systems). Another proposal has been put forward, which involves lithium cation migration toward the outside of the solid state oxide layer,[10,13] resulting in an insulator-to-metal transition of the oxide layer. The present study resolves unambiguously this issue: using secondary ion mass spectroscopy (SIMS), outstanding spatial images of chemical elements have been obtained, which allow for the 3D mapping of the lithium migration out of Li_xCoO_2. Moreover, the observed temperature dependence of the high resistance state (HRS) and low resistance state (LRS) of the devices reveals the changes of film properties, which are very well correlated with the migration (intercalation/deintercalation) of the lithium ions. Besides, a simple numerical model enables deciphering of the strong influence of electrode surface area on the switching kinetics, and hence extrapolation of the switching time down to 20×20 nm^2 devices.

2. Resistive Switching Mechanism

In the case of an E1/Li_xCoO_2/E2 device for which the E1/Li_xCoO_2 contact is of atomic size (**Figure 1**a, referred to as first configuration), the mechanism has been previously identified:[13] it involves the redox reaction of the cobalt of the film, coupled with that of the water meniscus. In the case of electrodes whose lateral size is greater than the thickness (≈100 nm) of the film (Figure 1b, denoted second configuration), the mechanism appears however "inverted," which may seem paradoxical: for the same negative polarization of the lower electrode, the film becomes locally less conducting in the first configuration, and more conducting in the second one.[13] Furthermore, it had been formerly observed that no forming voltage was needed,[8] thus no dramatic influence of moisture had been detected at first.[15] Hence, in the second configuration, which corresponds to the complete structure of a solid-state battery,[16] another RS mechanism had to be explored. One of the mechanisms proposed assumes that the devices behave like ECM for which the cations are reduced inside the oxide, forming metal filaments.[14] Another mechanism proposed assumes that lithium ions migrate out of the oxide film and are reduced in the doped Si electrode.[13] Simultaneously, the decreasing lithium stoichio metry (x) of Li_xCoO_2, which corresponds to the oxidation of the cobalt ions, leads to an increase of the film conductivity.[17]

Although transmission electron microscopy (TEM) is a useful method to observe the mechanisms for ECM (involving metal cations[18–22]), valence change memories,[23] and thermochemical unipolar systems,[24,25] it requires sample thinning processes,[18] which may partly destroy the regions of interest and thus prevent detailed spatial studies of the light Li^+ cations. Thus, SIMS is chosen here as the technique to study the elements composing Li_xCoO_2. Apart from obtaining depth profiles of elements, this technique allows, through recent enhancements, 2D composition maps,[26,27] and even 3D spatial distribution of chemical elements[28] in devices (see Section S1 in the Supporting Information).

In the studied Au/Li_xCoO_2/Si cells (Figure 1c), the films consist of columnar grains whose mean c-axis orientation is parallel to the substrate. We studied such devices by SIMS in the following configurations: i) virgin devices, ii) devices after a SET operation (RS from an initial HRS to a LRS), and iii) devices after a SET–RESET operation (SET operation followed by a RS back to a HRS).

In virgin devices (reproduced on 12 devices), lithium content in Si appears very low (see black arrow in SIMS profile, **Figure 2**a) and its 3D distribution appears fairly "uniform" (blue dots randomly distributed in Si, see Figure 2b). This corresponds to a "noise" signal attributed to the lower detection limit of the SIMS technique for this element. In contrast, in all preswitched devices (having undergone a SET operation, see Figure 2c left), 3D spatial distribution maps of lithium show several zones of higher lithium concentration in Si. These zones appear in the form of "carrots," measuring a few micrometers in diameter and a few hundred nanometers in depth. A typical example is illustrated in Figure 2d (two zones of lithium accumulation). The lithium composition found in these zones is over 20 times higher than in the surrounding zones ("noise" signal). Hence, this is clear evidence of lithium migration out of the film and into the silicon substrate. The Li_xCoO_2/Si interface is composed of a SiO_2 layer,[13] whose morphology (nonuniform thickness, presence of defects etc.) may control where lithium ions reach the Si surface and thus create the "carrot-shape" structure. On the contrary, devices studied by SIMS after a SET–RESET operation show little or no local accumulation of lithium in the silicon substrate (see Section S2 in the Supporting Information), which indicates the reintercalation of almost all lithium ions.

This local migration of lithium out of Li_xCoO_2 must be accompanied by a depletion of lithium inside the film. Nonetheless, this depletion is negligible compared to the initial lithium content in the film, since no difference in composition has been observed by SIMS compared to virgin film zones of the same studied samples. However, this slight lithium concentration decrease appears to be sufficient to modify the electrical properties of the films. To study and illustrate this effect, we measured the overall conductivity of devices as a function of temperature. For a given resistance state of a device, the current flowing across the cell was measured as a function of temperature T, using a low bias voltage (0.1 V). It is therefore possible, for the same device, to plot the conductivity

Dr. R. Salot
Laboratoire Microbatteries Embarquées
CEA de Grenoble
17 Avenue des Martyrs
38054 Grenoble, France

© 2018 WILEY-VCH Verlag GmbH & Co. KGaA, Weinheim

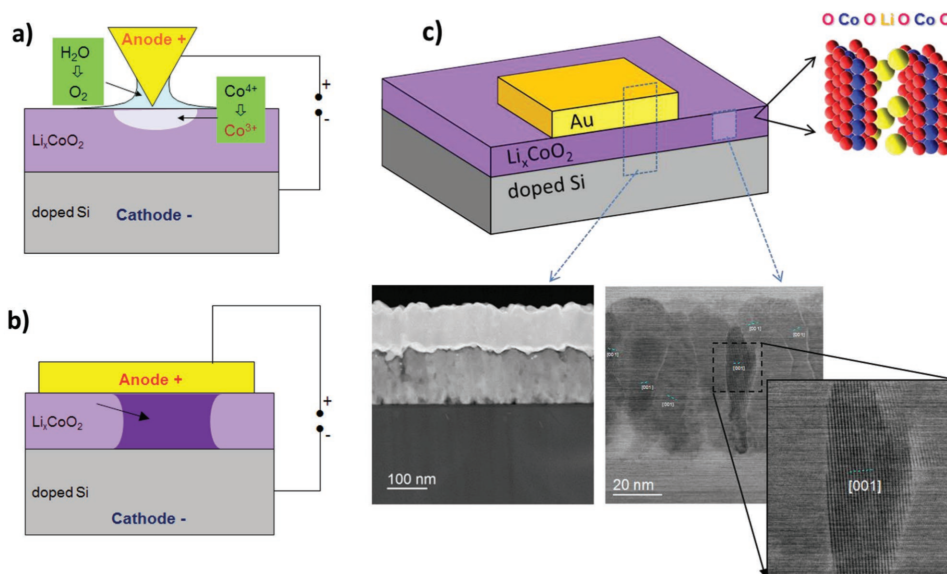

Figure 1. a) Schematic diagram of the mechanism in the case of an atomic contact between a conducting AFM tip and a Li_xCoO_2 film on a doped Si substrate: if the lower electrode is negatively biased, water (from the capillary meniscus) is oxidized and cobalt is reduced, yielding a less conducting zone (horizontal arrow). b) Schematic diagram in the case where the upper electrode lateral size is larger than the film thickness, for a lower electrode negative polarization: in such a case, it was previously observed that the oxide film becomes locally more conducting (dark colored zone, black arrow). c) Schematic view of the cells studied: the upper electrode is composed of a 100 nm gold layer deposited by thermal evaporation; TEM image (bottom left) of the Au/Li_xCoO_2/Si cell and TEM image (bottom right) of the film, consisting of grains with a *c*-axis overall parallel to the substrate surface.

as a function of $1000/T$, for several resistance states (initial state or HRS, then resistance states after 1, 2, or 3 successive SET pulses and then after a RESET operation) as illustrated in **Figure 3**. We can observe that the initial state corresponds to a semiconductor state (thermally activated with an activation energy of about 0.19 eV) and that, after each SET operation, the device conductivity increases significantly (from about 10^{-4} S cm^{-1} initially to 10^{-1} S cm^{-1}, at room temperature), and the corresponding curves become progressively more flat. This indicates a transition toward a more metallic or pseudometallic behavior,[17] which is well correlated with the evolution of the stoichiometry x of Li_xCoO_2 reported in the field of batteries: for $x \geq 0.94$, Li_xCoO_2 is a semiconductor whereas for $x \leq 0.75$, it is a metal.[17,29,30] In addition, it is also evident that a RESET operation reverts the device almost to its initial behavior. Such a mechanism of lithium deintercalation/intercalation from Li_xCoO_2 may appear advantageous, since it involves only very weak structural transformations.[11] Hence it may have an associated advantage to avoid undesired issues specifically encountered by ECM scaling down devices.[31,32] This could potentially lead to a better reversibility of the RS process, and thus to improvement of the write/erase endurance.

3. Resistive Switching Kinetics and Write/Erase Endurance

Very preliminary results had made it previously possible to point out a strong influence of the cell surface area on the switching kinetics of the devices.[13] Here, we have been able to study this kinetics in a much more precise way, and, additionally, to propose a model which can account, at least qualitatively, for the observed results. The experimental scheme used is illustrated in **Figure 4**a.

Pulse trains are applied between the lower electrode (doped-Si) of a metal–insulator–metal (MIM) cell and an atomic force microscope (AFM) conducting tip in contact with the upper electrode. After each set of (−8 V, 30 ms) pulses, the resistance of the device is measured using a low read voltage. The resistance of the device progressively decreases as a function of the number of pulses (of negative polarity), which follows the switching kinetics of SET (the kinetics of RESET, which was found much faster than the kinetics of SET, is not studied here, since a similar trend is observed in other systems[33]).

For modeling purposes, the MIM cell structure has been represented by a simple electrical circuit, as shown in Figure 4b. V_S corresponds to an external voltage source (delivering bias pulses) which is applied to the whole circuit. Resistance R_0 represents the total resistance of the {AFM lever + internal resistance of the measurement unit} system, taken as 10^4 Ω. The electrode/film/electrode cell itself is represented by a resistance R (to measure) in parallel to a capacitor C (corresponding to the electrodes' capacity), and u is the voltage, which appears across the cell (if $R >> R_0$, then $u \approx V_S$, otherwise u is smaller than V_S in absolute value). The blue-colored part of the subcircuit corresponds to an electrochemical cell whose current i_{ch} (considered negligible compared to the other currents) causes the modification of R. Thus, in a volume Vol = $d.S$ located between the electrodes (S being the upper electrode surface area and d the film thickness), we assume that a fraction part (α.Vol with α a parameter considered as roughly constant) undergoes a small modification dx of film stoichiometry, proportional to i_{ch}.dt. This results in the following expression, using a proportionality constant K_1

© 2018 WILEY-VCH Verlag GmbH & Co. KGaA, Weinheim

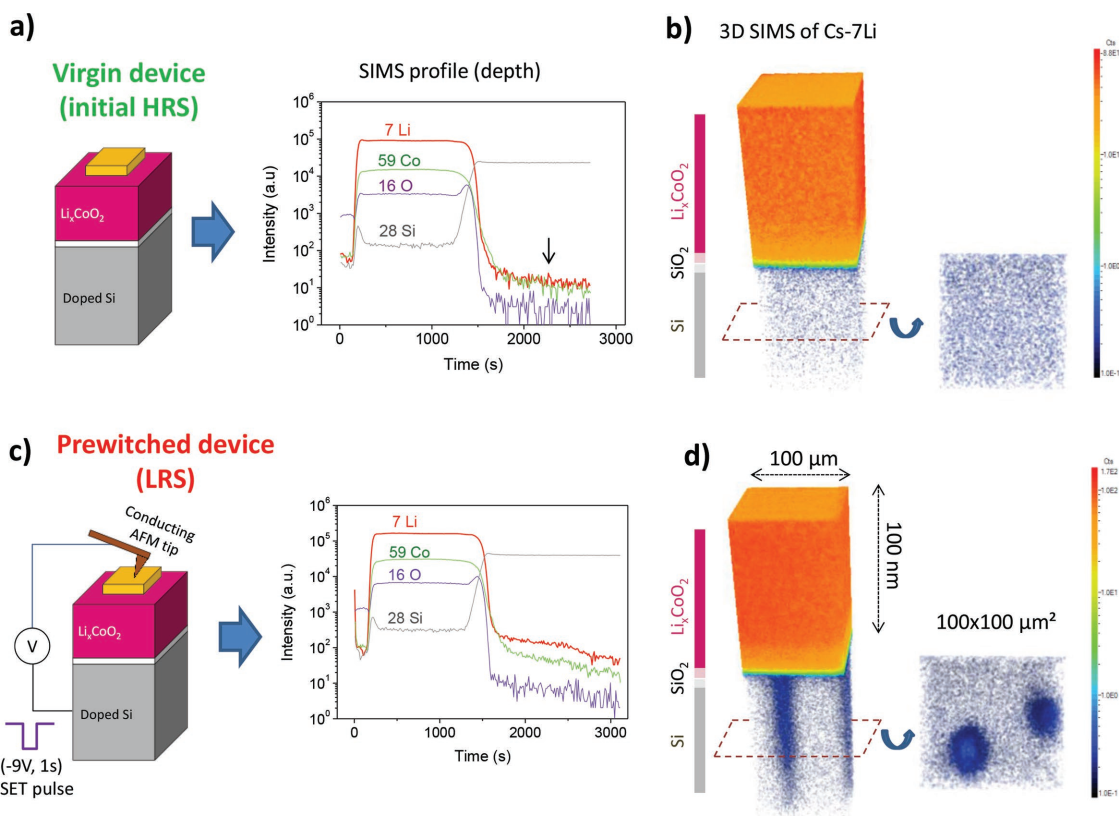

Figure 2. a) Left: schematic view of a virgin device (no RS carried out), Right: corresponding SIMS depth profile (volume analyzed: 100 × 100 µm^2 and 0.2 µm depth) of Cs-7Li, Cs-59Co, Cs-16O, and Cs-28Si. b) Left: corresponding Cs-7Li 3D distribution in the virgin cell (film/doped Si); inside the Si substrate, the Cs-7Li concentration appears low (blue dots) and randomly distributed (the absence of Li is white colored), Right: cumulative counts of Cs-7Li inside the Si substrate, projected on a horizontal plane. c) Schematic view (left) of a preswitched device (RS from HRS to LRS, due to a SET operation, using an AFM tip in contact with the upper Au electrode), and corresponding SIMS depth profile of Cs-7Li, Cs-59Co, Cs-16O, and Cs-28Si. d) Left: corresponding Cs-7Li 3D composition distribution in the preswitched cell (film/doped Si): "carrots-shaped" zones of higher Li concentration are observed. Right: cumulative counts of Cs-7Li inside the silicon substrate, projected on a horizontal plane. Two discoid zones (≈20 µm in diameter) of higher Cs-7Li concentration are clearly observed.

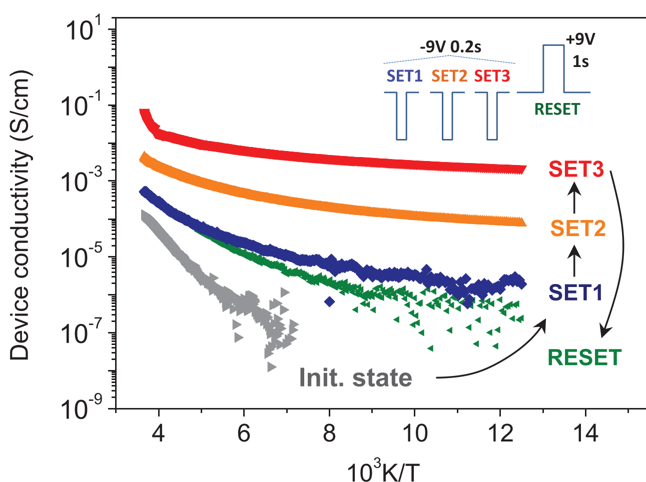

Figure 3. For a 100 × 100 µm² device, cell conductivity as a function of reciprocal temperature 1000/T (T varies from 298 K down to 80 K and back to 298 K with a rate of 20 K min^{-1}), for an initial state of the device (gray points), then after consecutive SET operations (blue, orange, and red points, see inset for pulse details) and finally after a RESET operation (green points).

$$\alpha.\mathrm{Vol}.\mathrm{d}x = K_1.i_{\mathrm{ch}}.\mathrm{d}t \Rightarrow \mathrm{d}x = \frac{K_1.i_{\mathrm{ch}}.\mathrm{d}t}{\alpha.\mathrm{Vol}} = \frac{K_1.i_{\mathrm{ch}}.\mathrm{d}t}{\alpha.d.S} \tag{1}$$

Besides, for simplification purposes, i_{ch} is assumed to have a roughly li near correlation to $u - V_{\mathrm{th}}$, where V_{th} is a threshold voltage below which (in absolute value) no modification occurs (V_{th} has been found experimentally to lie around –4 V for a SET operation). Thus, i_{ch} can be written, using a K_2 constant

$$i_{\mathrm{ch}} = K_2 .(u - V_{\mathrm{th}}) \tag{2}$$

Additionally, we assume an exponential dependence of the film resistivity ρ as a function of the stoichiometry x (ref. [17]) in the [0.85–0.98] range, using the K_3 and K_4 constants

$$\rho = K_3.\mathrm{e}^{K_4.x} \tag{3}$$

Since the total resistance of the cell follows the same law as the resistivity, we thus obtain

$$\frac{\mathrm{d}R}{R} = \frac{\mathrm{d}\rho}{\rho} = K_4.\mathrm{d}x = K_4.\frac{K_1.K_2.(u - V_{\mathrm{th}}).\mathrm{d}t}{\alpha.d.S} \tag{4}$$

© 2018 WILEY-VCH Verlag GmbH & Co. KGaA, Weinheim

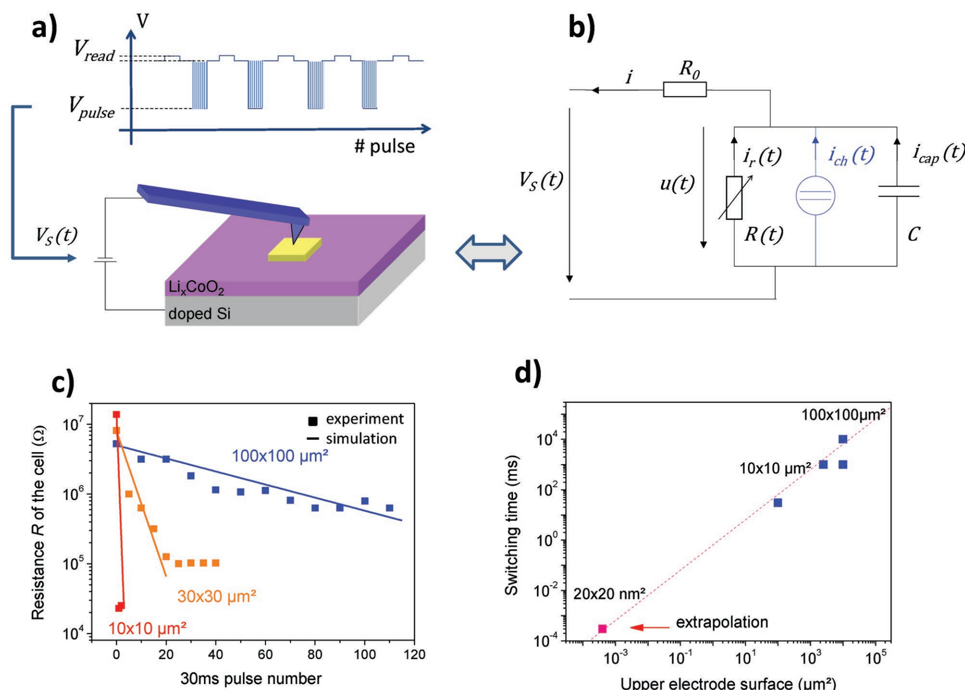

Figure 4. a) Schematic view of an {AFM tip–MIM cell} system, to which pulse trains (–8 V, 30 ms) are applied (in the experiment, the bias is applied to the bottom electrode, respectively to the AFM tip). After each train of pulses, the cell resistance is measured (at +1 V). b) Corresponding electrical circuit consisting of a resistance R (cell resistance), an electrochemical cell, and a constant capacitor C (electrodes) connected in parallel, and a resistance R_0 (tip-lever resistance + measurement unit resistance) connected in series with the "RC" subcircuit. All elements (except R_0 and C) are time-dependent, as specified. c) Cell resistance as a function of pulse number, for cells of different upper electrode sizes (100×100 µm^2, 30×30 µm^2, and 10×10 µm^2). d) Using the numerical simulation, the device switching time is plotted as a function of cell area (red-dotted line); experimental switching times measured using a single bias pulse (blue squares); extrapolation of HRS-LRS switching time down to 20×20 nm^2 (red square).

Finally, this leads to the following expression, using only one K constant

$$\frac{\mathrm{d}R}{R} = \frac{K.(u - V_{\mathrm{th}}).\mathrm{d}t}{S} \tag{5}$$

The remaining set of equations is related to the external electrical parameters (V_S, C, and R_0)

$$i_r = \frac{u}{R},\ i = \frac{V_S - u}{R_0},\ i_{\mathrm{cap}} = i - i_r,\ \frac{C.\mathrm{d}u}{\mathrm{d}t} = i_{\mathrm{cap}} \tag{6}$$

Utilizing Equations (5) and (6), a numerical simulation has been developed in order to obtain the time evolution of R, and thus the R decrease, as a function of the number of pulses. This has been done by a programmed loop in which time t is incremented by a small amount dt, and by computing all the parameters (i_r, i, i_{cap}, u, R) for each numerical value of t. The C value has been taken proportional to surface area S, neglecting the possible variation of the dielectric constant with the stoichiometry x.

The experimental results (Figure 4c) show that the cell surface area not only plays an extremely important role, but also that this resistance decrease is well approximated by the simulation (the only constant K of the model has been adjusted using $S = 100 \times 100$ µm^2). Indeed, a good qualitative agreement of the model with the experimental points is observed. This numerical simulation also allows to plot the device switching time (ST) (sum of pulse durations, determined to obtain a HRS/LRS ratio $\geq 10^2$) as a function of device area (Figure 4d, red-dotted line). This shows that the ST is slow for large surfaces (≈10 s for 100×100 µm^2 devices), but becomes much faster for smaller ones. Experimental results (Figure 4d blue squares) for the ST show a qualitative good agreement with the simulation. Using this model, we extrapolate the switching time to 20×20 nm^2 cells (Figure 4d red square). For such size, the switching time is predicted to reach about 100 ns. Despite the clearly established trend between switching time and cell surface area, as well as its corroboration by simulation, verifying the extrapolation of switching time for very low cell surface areas is a significant remaining issue to study for actual applications.

Concerning retention issues, preliminary results have been obtained concerning time stability of LRS and HRS resistances of cells at high temperature (130 °C under vacuum, see Section S3 in the Supporting Information). No resistance changes could be noticed after 1 h at such high temperature. The observed stability of the LRS may be attributed to the fact that Li can yield stable Li–Si compounds inside the Si electrode.[34]

Finally, we have obtained results of endurance, which appear also very promising. Cells of 500×500 µm^2 only sustain a few hundred cycles (not shown here) after which a very low resistance value is finally reached (the electric field applied is too low to allow switching back to a HRS). On the contrary, smaller cells of 10×10 µm^2 far exceed 5000 cycles (see **Figure 5**). This may be attributed to the fact that the probability of presence of

© 2018 WILEY-VCH Verlag GmbH & Co. KGaA, Weinheim

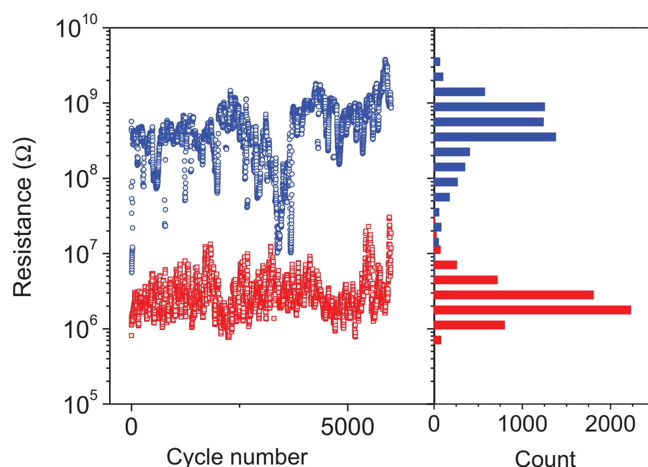

Figure 5. Example of HRS and LRS values as a function of cycle number, recorded on a 10 × 10 µm^2 device (read voltage +1 V). The endurance reaches beyond 5000 cycles with a HRS/LRS ratio ≈10^3.

film defects decreases with the downscaling of the cells. This also underlines that RS endurance here far exceeds the usual cycling life of lithium-ion batteries (≈1000 cycles).[35] The RS mechanism determined in our Li_xCoO_2 cells appears similar to charge–discharge mechanisms involved in the field of energy storage in batteries,[16] where the limitation of cycling life comes mainly from mechanical stresses (volume change) due to lithium incorporation in Si. Thus the endurance of Li_xCoO_2-based memories may at first sight also be limited by the usual cycling life of batteries. This not being the case (Figure 5), indicates that the quantity of lithium involved in RS may be much lower than in the usual complete charge–discharge process of lithium-ion batteries. Hence, much higher endurance should be reachable and will constitute the subject of future investigation, toward the need of >10^7 write/erase cycles in memory devices. In particular, the precise influence of moisture on kinetics[15] and endurance will be examined.

4. Conclusion

In conclusion, through 3D chemical element characterization, SIMS technique has proven to be a very powerful means to provide direct evidence of outward lithium migration from Li_xCoO_2 films into the silicon electrode. Moreover, the associated semiconductor-to-metal transition has been observed through conductivity measurements as a function of temperature in the 80–298 K range. Besides, the numerical model proposed accounts well for the high influence of the electrode surface area on the RS speed, which is predicted to reach around 100 ns for 20 × 20 nm^2 devices by numerical extrapolation. Furthermore, the endurance performance of films increases with downscaling (>5000 cycles for 10 × 10 µm^2 cells). Hence, attractive possibilities can be envisaged for this intercalation material class, and further work is ongoing, aiming to realize and study downscaling of the devices both toward nanometer scale memories and neuromorphic memristive devices. In particular, there are remaining significant issues to focus on, e.g., exploring the endurance and switching times down to the nanoscale, examining the precise influence of environment (moisture, vacuum) on the switching characteristics of cells, as well as investigating the resistance evolution of LRS and HRS with downscaling.

5. Experimental Section

Samples: Li_xCoO_2 thin films were deposited on degenerately doped p+-type Si (111) wafers by RF magnetron reactive sputtering (Alcatel SCM 600 apparatus) using a stoichiometric (x = 1) Li_xCoO_2 target, with an applied RF power of 500 W. The films were grown in a 3/1 Ar/O_2 (2.2 Pa) atmosphere and a bias of −50 V was applied to the substrate. The films (100 nm, as determined by a profilometer) were subsequently heated to 550 °C for 1 h in air in order to obtain the R-3*m* high-temperature (HT) Li_xCoO_2 phase.

Deposition of gold electrodes on Li_xCoO_2 films was performed by conventional Joule evaporation under secondary vacuum (1026 mbar). Nickel deposition masks, with various aperture sizes (≥10 µm) have been used.

Measurements: SIMS analyses have been carried out with a IMS7f CAMECA setup. The primary ion source used was composed of Cs^+ ions and the detected elements were of the M-Cs^+ type (both for depth profiles and 3D distributions), where M is a matrix element. A primary ion impact energy of 5 keV was used.

Cross-sectional TEM studies were carried out on Li_xCoO_2 samples using a Nion UltraTEM 200 scanning transmission electron microscope working at 60 kV. The samples were prepared for TEM by focused ion beam.

Electrical characterizations and modifications of Au/Li_xCoO_2/doped-Si cells were performed by (CP) AFM with a home-made system (Resiscope) for local contact resistances and current measurements, derived from a Multimode Nanoscope III AFM setup (Veeco).

Supporting Information

Supporting Information is available from the Wiley Online Library or from the author.

Acknowledgements

This work was supported, in part, by the Research Promotion Foundation of the Republic of Cyprus (Grant No. PENEK-0609-65), and by the French National Research Agency (ANR) as part of the “Investissements d'Avenir” program (Labex NanoSaclay, reference:ANR-10-LABX-0035). This paper is dedicated to Alec Moradpour, deceased in 2013, who had first the idea to look for the RS mechanism by means of SIMS. We are extremely grateful to him for all his ideas, advices and help. We are also very grateful to Prof. Alexandre Revcolevschi for fruitful discussions.

Conflict of Interest

The authors declare no conflict of interest.

Keywords

lithium-ion batteries, nonvolatile memories, oxides, resistive switching, thin films

Received: March 16, 2018
Revised: April 8, 2018
Published online:

© 2018 WILEY-VCH Verlag GmbH & Co. KGaA, Weinheim

[1] R. Waser, R. Dittmann, G. Staikov, K. Szot, *Adv. Mater.* **2009**, *21*, 2632.
[2] S. D. Ha, S. Ramanathan, *J. Appl. Phys.* **2011**, *110*, 071101.
[3] I. Valov, E. Linn, S. Tappertzhofen, S. Schmelzer, J. van den Hurk, F. Lentz, R. Waser, *Nat. Commun.* **2013**, *4*, 1771.
[4] G. S. Snider, *Proc. IEEE International Symposium on Nanoscale Architectures*, IEEE, Anaheim, USA **2008**, p. 85.
[5] R. Waser, M. Aono, *Nat. Mater.* **2007**, *6*, 833.
[6] A. Sawa, *Mater. Today* **2008**, *11*, 28.
[7] X. Zhu, C. S. Ong, X. Xu, B. Hu, J. Shang, H. Yang, S. Katlakunta, Y. Liu, X. Chen, L. Pan, J. Ding, R. W. Li, *Sci. Rep.* **2013**, *3*, 1084.
[8] A. Moradpour, O. Schneegans, S. Franger, A. Revcolevschi, R. Salot, P. Auban-Senzier, C. Pasquier, E. Svoukis, J. Giapintzakis, O. Dragos, V. C. Ciomaga, P. Chrétien, *Adv. Mater.* **2011**, *23*, 4141.
[9] J. D. Greenlee, C. F. Petersburg, W. G. Daly, F. M. Alamgir, W. A. Doolittle, *Appl. Phys. Lett.* **2013**, *102*, 213502.
[10] X. Zhu, J. Zhou, L. Chen, S. Guo, G. Liu, R. W. Li, W. D. Lu, *Adv. Mater.* **2016**, *28*, 7658.
[11] E. J. Fuller, F. El Gabaly, F. Léonard, S. Agarwal, S. J. Plimpton, R. B. Jacobs-Gedrim, C. D. James, M. J. Marinella, A. A. Talin, *Adv. Mater.* **2017**, *29*, 1604310.
[12] S. Wang, W. Wang, C. Yakopcic, E. Shin, G. Subramanyam, T. M. Taha, *Microelectron. Eng.* **2017**, *168*, 37.
[13] V. H. Mai, A. Moradpour, P. A. Senzier, C. Pasquier, K. Wang, M. J. Rozenberg, J. Giapintzakis, C. N. Mihailescu, C. M. Orfanidou, E. Svoukis, A. Breza, C. B. Lioutas, S. Franger, A. Revcolevschi, T. Maroutian, P. Lecoeur, P. Aubert, G. Agnus, R. Salot, P. A. Albouy, R. Weil, D. Alamarguy, K. March, F. Jomard, P. Chrétien, O. Schneegans, *Sci. Rep.* **2015**, *5*, 7761.
[14] Y. Y. Hong, in *Nanoscale Semiconductor Memories: Technology and Applications* (Eds: S. K. Kurinec, K. Iniewski), CRC Press, Taylor&Francis Group, Boca Raton, USA **2014**, Part VI, p. 396.
[15] a) M. Lübben, S. Wiefels, R. Waser, I. Valov, *Adv. Electron. Mater.* **2018**, *4*, 1700458; b) M. Lübben, P. Karakolis, V. Ioannou-Sougleridis, P. Normand, P. Dimitrakis, I. Valov, *Adv. Mater.* **2015**, *27*, 6202; c) T. Tsuruoka, K. Terabe, T. Hasegawa, I. Valov, R. Waser, M. Aono, *Adv. Funct. Mater.* **2012**, *22*, 70.
[16] N. Ariel, G. Ceder, D. R. Sadoway, E. A. Fitzgerald, *J. Appl. Phys.* **2005**, *98*, 023516.
[17] M. Ménétrier, I. Saadoune, S. Levasseur, C. Delmas, *J. Mater. Chem.* **1999**, *9*, 1135.
[18] Y. Yang, P. Gao, S. Gaba, T. Chang, X. Pan, W. Lu, *Nat. Commun.* **2012**, *3*, 732.
[19] W. A. Hubbard, A. Kerelsky, G. Jasmin, E. R. White, J. Lodico, M. Mecklenburg, B. C. Regan, *Nano Lett.* **2015**, *15*, 3983.
[20] F. Yuan, Z. Zhang, C. Liu, F. Zhou, H. M. Yau, W. Lu, X. Qiu, H. S. Philip Wong, J. Dai, Y. Chai, *ACS Nano* **2017**, *11*, 4097.
[21] M. J. Song, K. H. Kwon, J. G. Park, *Sci. Rep.* **2017**, *7*, 3065.
[22] Z. Xu, Y. Bando, W. Wang, X. Bai, D. Golberg, *ACS Nano* **2010**, *4*, 2515.
[23] L. Yao, S. Inkinen, S. van Dijken, *Nat. Commun.* **2017**, *8*, 14544.
[24] J. Yao, Z. Sun, L. Zhong, D. Natelson, J. M. Tour, *Nano Lett.* **2010**, *10*, 4105.
[25] J. Yao, L. Zhong, D. Natelson, J. M. Tour, *Sci. Rep.* **2012**, *2*, 242.
[26] S. G. Boxer, M. L. Kraft, P. K. Weber, *Annu. Rev. Biophys.* **2009**, *38*, 53.
[27] A. Cabin-Flaman, A. F. Monnier, Y. Coffinier, J. N. Audinot, D. Gibouin, T. Wirtz, R. Boukherroub, H. N. Migeon, A. Bensimon, L. Jannière, C. Ripoll, V. Norris, *Anal. Chem.* **2011**, *83*, 6940.
[28] Y. Fleming, T. Wirtz, *Beilstein J. Nanotechnol.* **2015**, *6*, 1091.
[29] J. N. Reimers, J. R. Dahn, *J. Electrochem. Soc.* **1992**, *139*, 2091.
[30] T. Motohashi, Y. Katsumata, T. Ono, R. Kanno, M. Karppinen, H. Yamauchi, *Chem. Mater.* **2007**, *19*, 5063.
[31] S. Ambrogio, S. Balatti, A. Cubeta, A. Calderoni, N. Ramaswamy, D. Ielmini, *IEEE Trans. Electron Devices* **2014**, *61*, 2920.
[32] T. Ninomiya, S. Muraoka, Z. Wei, R. Yasuhara, K. Katayama, T. Takagi, *IEEE Electron Device Lett.* **2013**, *34*, 762.
[33] N. Ghenzy, M. J. Sanchez, M. J. Rozenberg, P. Stoliar, F. G. Marlasca, D. Rubi, P. Levy, *J. Appl. Phys.* **2012**, *111*, 084512.
[34] H. Kim, C.-Y. Chou, J. G. Ekerdt, G. S. Hwang, *J. Phys. Chem. C* **2011**, *115*, 2514.
[35] G. Ning, B. N. Popov, *J. Electrochem. Soc.* **2004**, *151*, A1584.

© 2018 WILEY-VCH Verlag GmbH & Co. KGaA, Weinheim